Internal erosion by suffusion on cohesionless gap-graded soils: Model and sensibility analysis

Rachel Gelet, Didier Marot

Internal erosion by suffusion on cohesionless gap-graded soils: model and sensibility analysis

Rachel Gelet[a,*], Didier Marot[a]

[a]*Institut GeM, UMR CNRS 6183, Université de Nantes, 44600 Saint-Nazaire, France*

Abstract

Cohesionless gap-graded soils are susceptible to volumetric internal erosion, also called suffusion, under the action of seepage flow through the porous material. More precisely, during suffusion three processes simultaneously take place: detachment, transport and possible filtration of the fine particles. This paper proposes a new relationship to describe the development of suffusion based on the energy approach. The proposed relationship is a power law that relates the volumetric cumulative eroded mass with the volumetric cumulative energy dissipated by the flow. This law requires three material parameters: the erosion resistance index and the maximum volumetric cumulative energy that both characterize the fully-eroded state; and a smoothing time that controls the suffusion kinetics. The first two parameters are being measured from a series of experimental tests performed in oedometric conditions. The experimental program was set up to study suffusion development on three different soils and along three seepage lengths. The erosion resistance index was found to be insensitive to the seepage length. On the other hand, the maximum volumetric cumulative energy tends to increase with the seepage length. This increase is being attributed to the transport and filtration phenomena. The cumulative eroded mass predicted by the energy-based relationship compares reasonably well with the experimental data, by fitting for each test a fixed smoothing time. To improve our physical understanding of the suffusion kinetics, a relationship between the smoothing time and the hydraulic diffusion time is postulated in accordance with experimental observations. Such hypothesis improves the cumulative eroded mass predictions.

Keywords: internal erosion, suffusion, erodimeter, energy-based approach, erosion resistance index, flow power

1. Introduction

The management of earth dams and levees is a major operational concern for powerplant operators and stakeholders since they have to guarantee the stability and the operational function of these structures to regulatory authorities. Water seepage within earth structures can induce a detachment and a migration of fine particles from the soil structure itself or its foundation. This phenomenon called internal erosion has been distinguished in four types [8]: concentrated leak erosion, backward erosion, contact erosion and suffusion. This paper deals with the suffusion process, also called internal instability, which takes place inside the soil matrix. At the scale of a representative elementary volume (REV), suffusion embraces three simultaneous processes: detachment, transportation and partial filtration of the fine particles within the constrictions of the granular skeleton of the coarse fraction.

The surveillance of hydraulic structures with respect to suffusion raises four needs: the evaluation of the likelihood of suffusion initiation [17, 5], the localisation within a structure of the potential weak zones [38, 36], the study of the suffusion process initiation and progression [20, 32, 14] and the mechanical consequences of suffusion [30, 22, 27, 37, 1].

*Principal corresponding author

Email addresses: rachel.gelet@univ-nantes.fr (Rachel Gelet), didier.marot@univ-nantes.fr (Didier Marot)

Several geometric methods have been proposed to evaluate the likelihood of suffusion, either based on the grain size distribution [13, 35, 6] or on the constriction size distribution [11]. Although conservative [17, 35] and sometimes contradictory [26, 40], these methods have proven to be useful in practice as first screening tools. The localisation within a large structure of zones susceptible to suffusion requires a large amount of data usually gathered during the construction [38, 36]. Since those methods inherit the limitations encountered at the laboratory scale, they call for a cautious use.

Once the likelihood of suffusion is raised, the progression of the suffusion phenomenon needs to be tackled. The description of the progression of suffusion requires to link the soil response to the relevant hydraulic loading. On one hand, the scientific community agrees that the soil response is well described by the rate of eroded mass or by the cumulative eroded mass, i.e. at the scale of a REV the mass collected at the outlet of the soil volume. On the other hand, no consensus has been reached on the nature of the relevant hydraulic loading. The hydraulic loading on soil particles is often described by four distinct approaches: the hydraulic gradient [21], the hydraulic shear stress [24, 39], the pore velocity [34, 23] and the power dissipated by the flow [19, 32, 4]. Owing to its definition, suffusion may be accompanied by the filtration of some detached particles causing a redistribution of the porosity, particle size distribution and hydraulic conductivity, and *in fine* a redistribution of the local pore pressures or flow rates. Hence, both the imposed hydraulic load, (either the pore pressure/head/hydraulic gradient or the flow), and the local hydraulic response (respectively the flow rate or the pore pressure/head/hydraulic gradient) should be accounted for to compute the relevant hydraulic loading. With this respect, the hydraulic shear stress that is expressed in terms of pressure gradient, porosity and intrinsic permeability, and the power dissipated by the flow that is the product of the hydraulic head with the flow rate obey this condition. Moreover, the rate of eroded mass may decrease with time [25] or oscillate [32] so that the linear increase of the rate of eroded mass with the hydraulic shear stress proposed by Reddi et al. [24] is unlikely to be robust towards all hydraulic loading paths.

Finally, several triaxial tests have been performed to investigate the effect of suffusion on the mechanical behaviour of tested soils [7, 12] and various constitutive models have been proposed involving multiscale approaches [30], critical state based models [22, 37] and characteristic state based model [27, 28]. Although, the consequences of suffusion on the mechanical behaviour and properties of soils remain to date an open question [1], it is informative to highlight that these models often use the porosity induced by suffusion as an input to drive their mechanical constitutive models.

With the aim to describe the progression of suffusion, a series of tests was performed on gap-graded soils with three different fine particle contents. Two experimental devices are being used to tackle three seepage lengths. To consider various loading histories, the applied hydraulic gradient for each test was increased by stages according to different values of amplitude and duration. Within the framework of the energy approach [19], each test is being pursued up to a stable state of suffusion characterized by a constant hydraulic conductivity and a decreasing erosion rate. At this stable state of suffusion, the erosion resistance index and maximum volumetric cumulative energy are computed and the influences of the percentage of fine particles and specimen length are investigated. Based on this stable state of suffusion, the progression of suffusion is described by the energy-based approach [14]. The relevant hydraulic loading is characterized by the volumetric cumulative energy that is the integration over time of the volumetric power expended by the flow and the corresponding erosion is characterized by the volumetric cumulative eroded mass. This approach uses three material parameters: the erosion resistance index, the maximum volumetric cumulative energy and a smoothing time. A sensitivity analysis is carried out on the smoothing time that controls the kinetics of suffusion and a link between this parameter and the diffusion time is postulated.

2. Experimental devices and test procedure

To validate the suffusion law that will be presented in Section 4, the eroded mass prediction will be compared against several laboratory suffusion tests. In fact, suffusion has been experimentally investigated in the past [40] with tests on two different apparatuses, so that three specimen sizes could be tested. The two experimental devices are designed to apply a downward seepage flow. The first device is a triaxial erodimeter cell (T), under which several tests were performed and interpreted by Le et al. [16]. The second

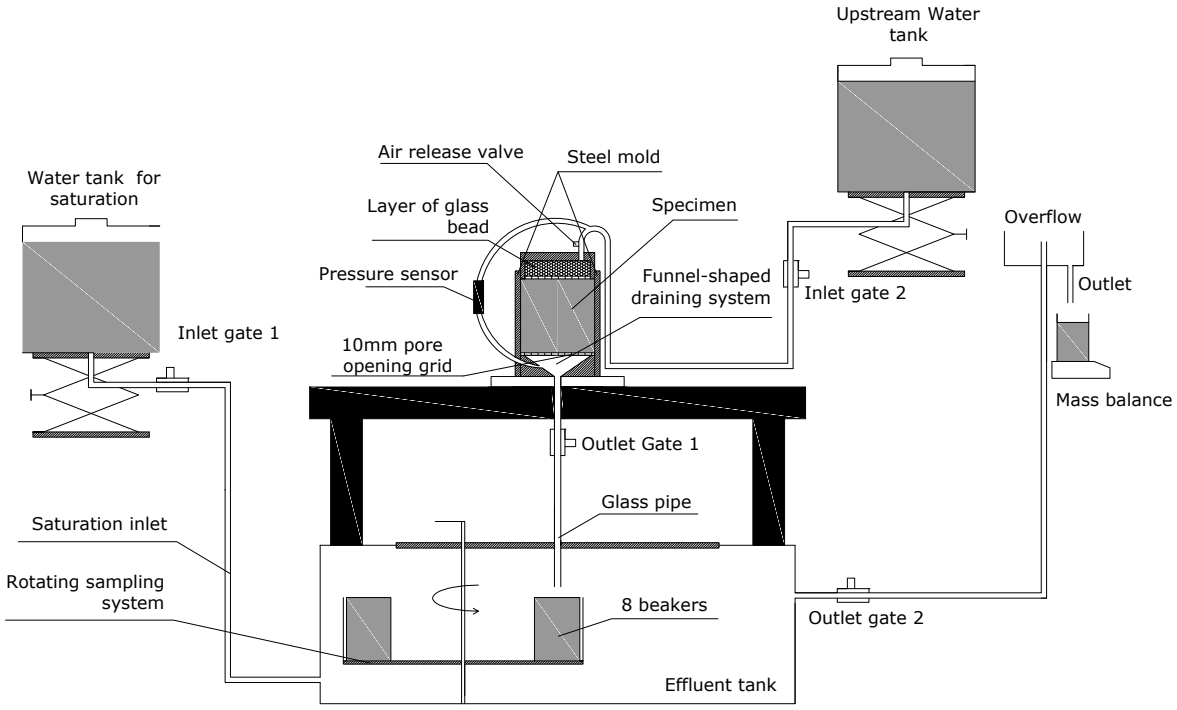

Figure 1: Principle of the triaxial erodimeter cell, collecting system and hydraulic control system.

is an erodimeter with a rigid wall cylindrical cell, named oedopermeameter (O), under which companion tests were performed and interpreted by Zhong et al. [40]. The diameters of these devices are 50 mm and 280 mm, respectively. General illustrations are presented in Figures 1 and 2. A detailed description of each device was reported in [3] and [29], respectively; however, a brief summary is provided here. For both devices, the fluid circulates into the top cap, which contains a layer of gravel or glass beads to diffuse the fluid flow uniformly on the specimen top surface. Both cell bases have a vertical funnel-shaped draining system specially designed to avoid clogging. Each draining system is connected to a collecting system, which is composed of an effluent tank containing a rotating support with eight beakers to catch the eroded particles during testing. With the objective to test specimens in oedometric condition with both devices, the membrane of the triaxial erodimeter is surrounded by a steel mold. In both devices, the specimen is placed on a sieve with 1.2-mm pore opening size that is fixed on a 10-mm mesh screen. According to the apparatus used, the range of flow rate varies; thus, two configurations are required: a flowmeter is used in the case of the oedopermeameter, whereas at the overflow outlet of the triaxial erodimeter, water falls in a beaker that is continuously weighed. For both apparatuses, the differential pore water pressure across the specimen is measured using a differential pressure transducer connected to the top cap and the pedestal base.

Soils that are likely to suffer from suffusion have a grain-size distribution curve either discontinuous or upwardly concave [8]. For this work, three cohesionless soils with a gap-graded distribution were selected (see Figure 3). Soils 1 and 6 are composed of mixtures of sand and gravel marketed by Sablière Palvadeau in France; while soil 4 is a mixture of Fontainebleau sand and gravel. According to criteria based on the grain size distribution [13] or based on the constriction size distribution [11], these soils are potentially unstable (see Table 1). As the gap ratio Gr is smaller than 3 for soil 4, this soil is classified as internally stable by

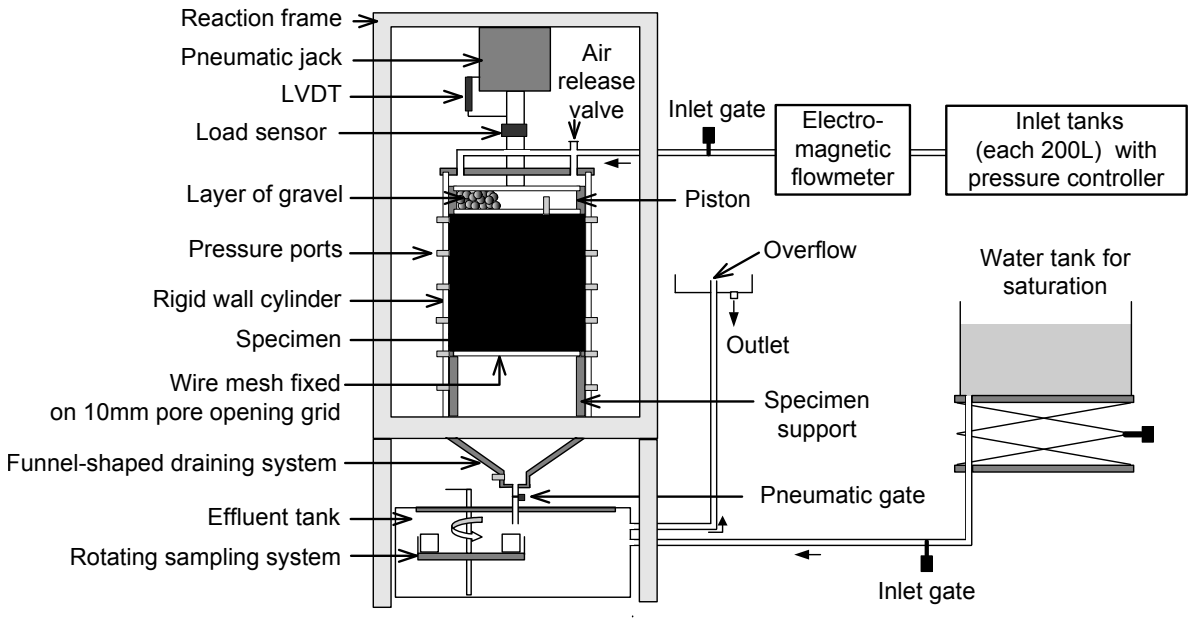

Figure 2: Principle of the oedopermeameter cell, collecting system and hydraulic control system.

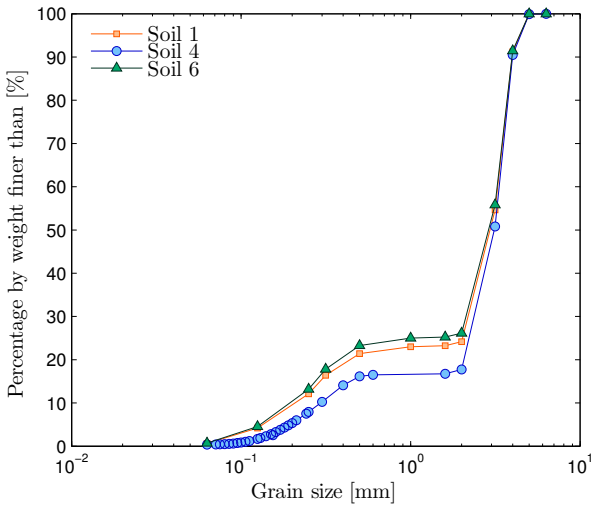

Figure 3: Grain size distribution of soils 1, 4 and 6.

Chang and Zhang's method [6].

Among the eleven prepared specimens, four of them were placed in the oedopermeameter cell in three layers and each layer was compacted in order to reach the initial fixed dry density. Seven specimens were prepared in the triaxial erodimeter device, using a single-layer semi-static compaction technique, in order to reach the target value of initial dry density 17 kN/m^3. The upward saturation of all specimens started by injecting carbon dioxide to improve the dissolution of gases into water and was completed by adding water.

With the objective to improve the readability, the first number of each test name is related to a soil gradation (Fig. 3). The letter indicates the used apparatus: O for the oedopermeameter cell and T for

Table 1: Properties of the tested gradations.

Gradation number	1	4	6
d_{15} (mm)	0.29	0.45	0.28
d_{50} (mm)	2.97	3.12	2.92
d_{60} (mm)	3.27	3.35	3.35
d_{90} (mm)	3.97	4.00	4.00
$D^c_{c35}/d^f_{85,SA}$	2.773	1.273	2.773
P (%)	0.64	0.36	0.70
Gr	1.60	2.67	1.60
C_u	15.70	11.17	16.75
$(H/F)_{min}$	0.125	0.094	0.120
$D(H/F)_{min}$	0.494	0.490	0.494
Finer KL (%)	23	16.5	25
Kenney and Lau [13]	Unstable	Unstable	Unstable
Chang and Zhang [6]	Unstable	Stable	Unstable
Indraratna et al. [11]	Unstable	Unstable	Unstable
e_{min}	0.56	0.56	0.53
e_{max}	0.63	0.73	0.58

Note: D^c_{c35} is the controlling constriction for the coarser fraction from the constriction size distribution by surface area technique; $d^f_{85,SA}$ is the representative size for finer fraction by surface area technique; P = percentage of particle smaller than 0.063mm; Gr = d_{max}/d_{min} (d_{max} and d_{min}: maximal and minimal particle sizes characterizing the gap in the grading curve); C_u = uniformity coefficient; F and H are the mass percentages of the grains with a size lower than a given particle diameter d and between d and 4d, respectively; $(H/F)_{min}$ is the minimal value of the ratio H/F; D $(H/F)_{min}$ is the corresponding diameter with the minimum value of ratio H/F; Finer KL is the corresponding fine percentage with the minimal value of ratio H/F; e_{min} and e_{max} are the minimal and maximal values of void ratio, respectively.

the triaxial erodimeter cell (used in oedometric conditions), and the last number specifies the specimen number. Table 2 indicates for the eleven tested specimens the length of the specimen, the initial dry density (post-saturation), the range of applied hydraulic gradient and the duration of each test. Each specimen is indeed subjected to a downward flow driven by a multi-step hydraulic gradient as shown in Figures 4 and 5. It is worth highlighting that for this experimental campaign, different histories of hydraulic loading were applied.

The response of each specimen is characterized by its hydraulic conductivity whose computation is based on Darcy's formula (Figures 4 and 5). Some of the tests would incur a decrease of hydraulic conductivity at the first stages of the erosion process, 6-O-1, or during the whole erosion process, 6-T-1 and 6-O-2. This decrease of hydraulic conductivity is attributed to some fine particles, detached and transported under the imposed water seepage and filtered within the soil itself. This filtration induces local clogging and thus a decrease of the hydraulic conductivity. The subsequent increase in hydraulic conductivity, such as in the case of 6-T-2 and 6-O-1, is due to the washing out of fine particles caused by much larger hydraulic gradients, overcoming the clogging aspect.

The soil response is also characterized by the experimentally measured cumulative eroded mass per unit volume of each specimen (symbols in Figures 10 and 11). Several beakers were used to catch the eroded particles during the saturation phase and during each hydraulic stage and the corresponding dry masses were measured. In a general manner, the eroded mass increases by steps [32], yet in our case the cumulated eroded mass for each step is displayed. This corresponds to the successive steps of the applied hydraulic gradient. These measured cumulative eroded masses form a reference to validate the energy-based approach

Table 2: Main characteristics of the tested specimens.

Test name	Specimen length (mm)	γ_d (kN/m^3)	i (-)	Tested duration (min)
1-T-1	50	16.93	0.4 - 3.0	180
1-T-2	100	16.98	0.07 - 0.95	165
1-O-1	435	16.22	0.042 - 0.237	134
4-T-1	50	16.96	0.1 - 1.5	150
4-T-2	100	16.99	0.043 -0.705	170
4-O-1	437	15.87	0.039 - 0.13	145
6-T-1	50	16.97	0.094 - 7.502	253
6-T-2	100	17.00	0.053 - 2.837	120
6-T-3	100	16.95	0.07 - 1.131	144
6-O-1	430	17.30	0.041 - 0.5	181
6-O-2	435	16.73	0.044 - 0.7742	310

Note: γ_d = post-saturation dry density; i = range of applied hydraulic gradient

(Section 4) to describe the kinetics of suffusion. For a given gradation, it is worth noting that the large discrepancy of the eroded dry mass per unit volume reflects the different micro-structures of the specimens induced by different amounts of lost mass during the saturation phase and different histories of applied hydraulic loading.

3. Energy-based approach and sensitivity analysis of the fully eroded state

Suffusion is the result of a seepage flow within a deformable porous medium and corresponds to the process of detachment, transport and filtration of the finest particles. With the aim to experimentally describe the phenomenon of suffusion, the soil response needs to be related to the hydraulic loading. Several results [24, 19, 32, 33] suggest that the fate of eroded particles, including particle re-deposition and pore clogging, significantly governs the internal erosion process. Hence, the appropriate hydraulic loading should account for *both* the external loading, such as the pressure gradient or the hydraulic gradient, and the soil's response, such as the seepage velocity or the hydraulic flow. In accordance, the energy-based approach represents the hydraulic loading by the power expended by the flow P_{flow} which is the product of the volumetric water flow rate Q by the differential head between the upstream and the downstream sections Δh and by the volumetric weight of water γ_w,

$$P_{\text{flow}} = \Delta h \times \gamma_w \times Q \,. \tag{1}$$

This expression was deduced from the energy conservation equation for the fluid phase and involves five assumptions [19]: (i) the energy is mainly dissipated by viscous shear at the direct vicinity of solid particles, (ii) the fluid temperature is constant, (iii) the system is adiabatic, (iv) a steady-state flow is considered, and (v) the flow is considered laminar.

Alike the eroded mass which is cumulated over time m_{cum}, the relevant hydraulic loading, i.e. the power expended by the flow, is integrated over time. Hence, the cumulative flow energy E_{cum} at the time t_i is defined as the time integration of the instantaneous flow power from the beginning of the test t_0,

$$E_{\text{cum}}(t_i) = \int_{t_0}^{t_i} P_{\text{flow}}(\tau)\,\mathrm{d}\tau \quad \text{with} \quad t_i > t_0 \,. \tag{2}$$

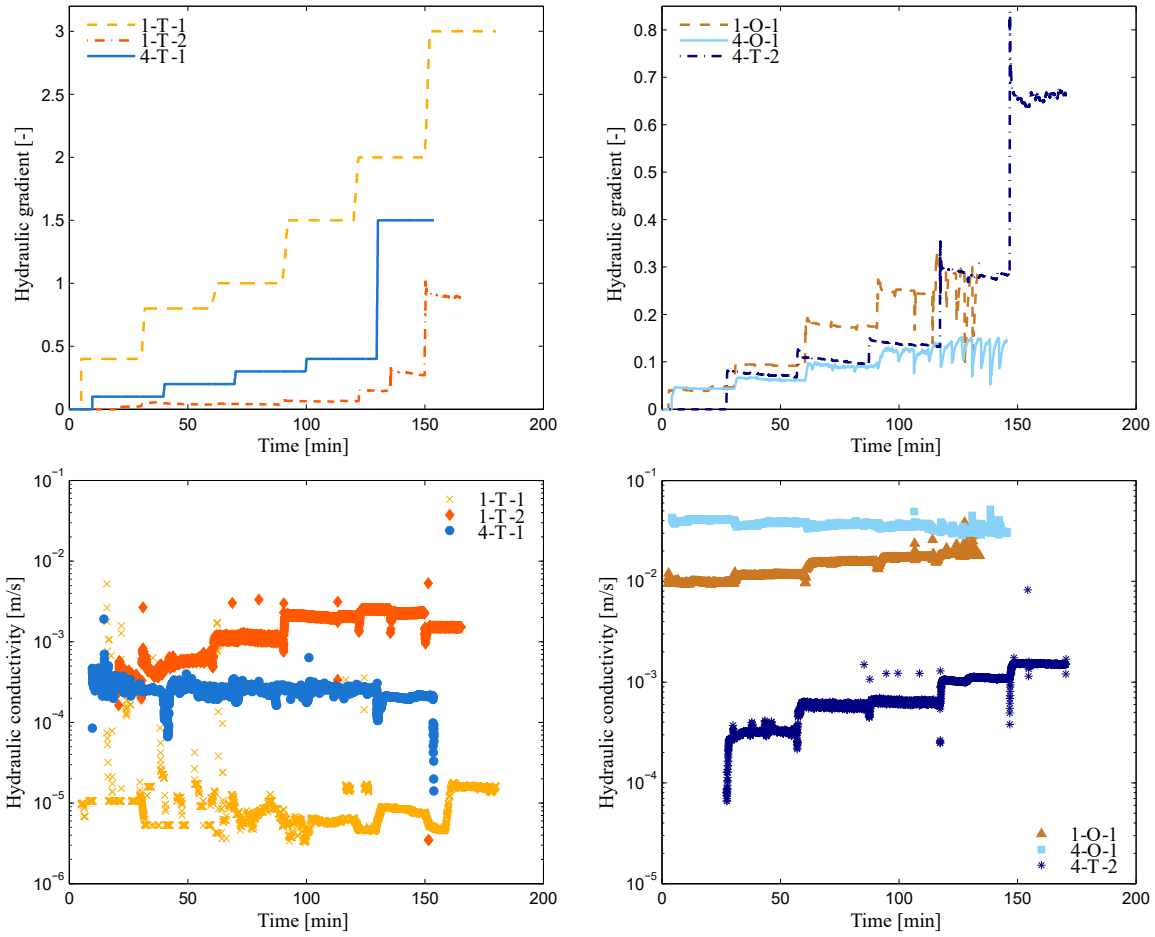

Figure 4: Time evolution of (top) the applied hydraulic gradient and (down) the measured hydraulic conductivity for specimens of soils 1 and 4.

While most approaches focus on the initiation of suffusion, the spirit of the energy-based approach [19] is to consider the whole development of the suffusion process. In fact, this approach assumes that the development of the suffusion process eventually reaches a stable state that corresponds to a fully eroded state. This assumption was made upon observing numerous experimental tests [25, 15, 40]. Recall that we obtain a fully-eroded state when the hydraulic conductivity becomes constant and the rate of eroded mass decreases or stabilizes at a low value, even if the hydraulic gradient is further increased. Note that if both conditions need to be met, they don?t need to be met simultaneously. Several examples regarding the identification of the fully-eroded state are highlighted in [26] and [40]. To make sure that the fully-eroded state has been reached, the time evolution of both the hydraulic conductivity and the rate of eroded mass are being plotted and the above conditions are searched. If the fully-eroded state has not been reached, the experimental test is redone with a different hydraulic loading path. Multi-staged hydraulic loading paths are preferred since they favor the occurrence of the fully-eroded state [26], see Figures 4 (top) and 5 (top). Aside from the metrology challenge, the main advantage of considering this fully eroded state is that it is fairly independent of the hydraulic loading path, as opposed to the initiation [26]. At this fully eroded state, the cumulative eroded mass is denoted $m_{\max}$ and the cumulative expended energy $E_{\max}$.

The method was primary developed to measure the suffusion susceptibility in the form of a suffusion resistance index I_α. With the objective to remain independent of the tested soil volume, the suffusion

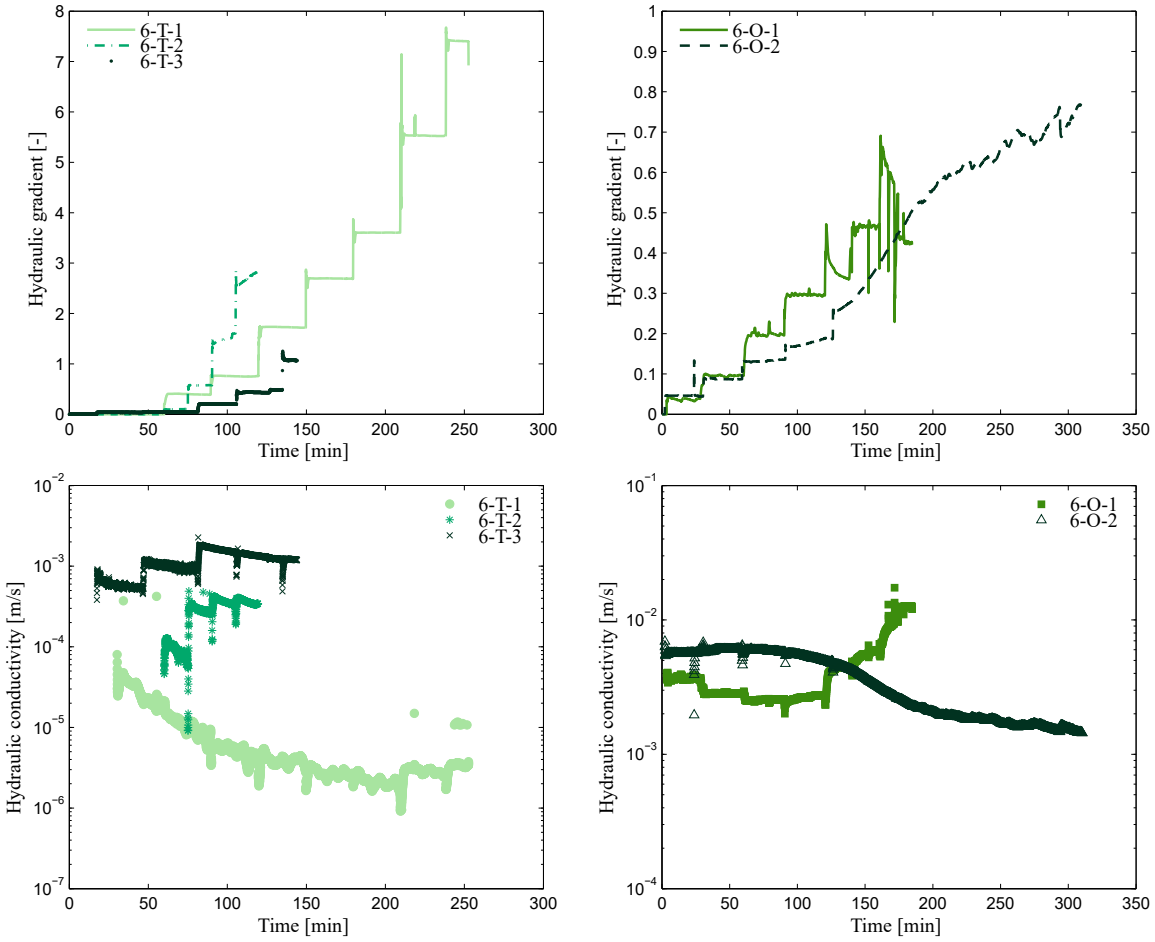

Figure 5: Time evolution of (top) the applied hydraulic gradient and (down) the measured hydraulic conductivity for specimens of soil 6.

susceptibility was obtained as a function of the ratio of the maximum cumulative eroded mass and the maximum cumulative expended energy,

$$I_\alpha = -\log\left(\frac{m_{\max}}{E_{\max}}\right) . \tag{3}$$

Based on an extended experimental campaign, in which twelve soils covering a large range of erodibility were subjected to one or several hydraulic loading paths, this suffusion resistance index I_α was observed to vary from highly erodible for $I_\alpha < 2$ to highly resistant for $I_\alpha \geq 6$. This classification brings a finer characterization of the erodibility [20] compared to the useful but rough classifications solely based on the grain size distribution [13, 35, 6].

The fully eroded state is characterized by two parameters: $E_{\max}$ and I_α. Yet, the volume of the soil that is eroded up to the fully eroded state influences the magnitude of $E_{\max}$ so that we prefer to work with the maximum cumulative expended energy *per unit volume* denoted $\bar{E}_{\max}$ and the maximum eroded mass *per unit volume* denoted $\bar{m}_{\max}$ (Figure 6). Throughout, the overhead bar will refer to a volumetric quantity. For each tested specimen, the fully eroded state corresponds to the upper-right point.

It is important to understand that the suffusion process and the fully eroded state are both very much influenced by the initial micro-structure of the specimen [16]. Based on a wide panel of 18 soils, Le et al.

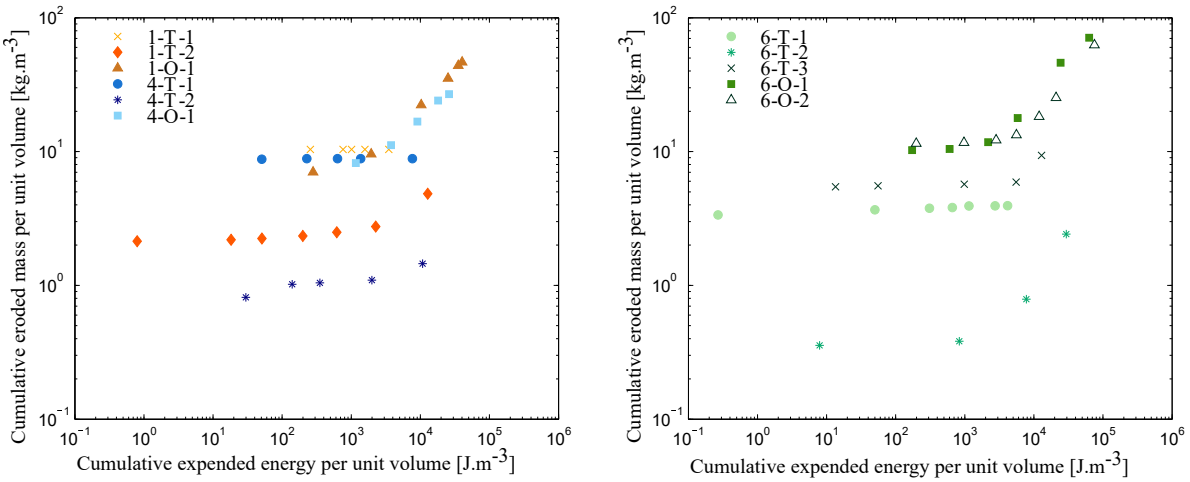

Figure 6: Cumulative eroded mass per unit volume versus cumulative expended energy per unit volume for the specimens of (left) soils 1 and 4 and (right) soil 6.

[16] evidenced that denser specimens tend to be more resistant to suffusion and conversely. It is worth noting that this conclusion does not apply to certain specific soils characterized by a large gap ratio and a low percentage of fines [31, 2]. The initial density (post-saturation and prior-suffusion) of each specimen tends to vary depending on the eroded mass lost during saturation. Although, the saturation process is performed with great care, to date we are not able to control the amount of eroded mass lost during the saturation phase, see for ex. specimens 6-T-2 and 6-T-3 in Figure 6, and hence we are not able to control the initial miro-structure accurately. This is one reason why repeatability results concerning suffusion tests are seldom presented. To take this issue into account, the two parameters describing the fully eroded state will be scrutinized upon scaling by the initial dry density of each specimen.

If parameters intrinsic to a tested material can be influenced by the initial micro-structure, they should not be influenced by the seepage length. Therefore, the deviation from the mean of two key parameters, $\bar{E}_{\max}$ and I_α, scaled by the dry density γ_d, is compared against the seepage length in Figure 7. For each soil, $\bar{E}_{\max}/\gamma_d$ tends to increase with the flow length. Indeed, the maximum volumetric cumulated energy $\bar{E}_{\max}$ dissipated by suffusion involves three mechanisms: detachment, transport and possible filtration of the fines particles. While the volumetric energy used for pure detachment should not be influenced by the flow length, it is expected that more volumetric energy be dissipated for the transportation of fines particles through a porous medium when the seepage length increases. The same is expected for the re-detachment mechanism. It should be noted that the least-square linear correlation is fairly good for the three soils presented, R^2 ranging between 0.93 and 1. Now for seepage lengths larger than 0.1 m, it is interesting to notice that the maximum volumetric cumulated energy increases with the initial percentage of fines particles (Figure 3). This dependence of $\bar{E}_{\max}/\gamma_d$ towards the seepage length and the initial percentage of fines particles should be broaden to other soils and seepage lengths as a future work.

Figure 7 (right) presents the deviation from the mean of I_α/γ_d against the seepage length. If the mean is assumed to represent the exact value, these results may be viewed as relative errors. Figure 7 (right) shows that the resistance index is not influenced by the flow length as also demonstrated by Zhong et al. [40] and by Kodieh et al. [14]. Yet, the relative errors are somewhat quite large, ranging from 3% to 30%, which indicates that the measurement of this parameter calls for a better accuracy. Indeed, the fully eroded state is reached when the hydraulic conductivity remains constant and the erosion rate decreases upon further increasing the hydraulic loading. Although, the hydraulic conductivity is being measured at a high frequency during the suffusion test, to date the eroded mass is only known several hours after the end of the suffusion test. Because of this metrology constraint, the accurate identification of the fully eroded state remains to be improved.

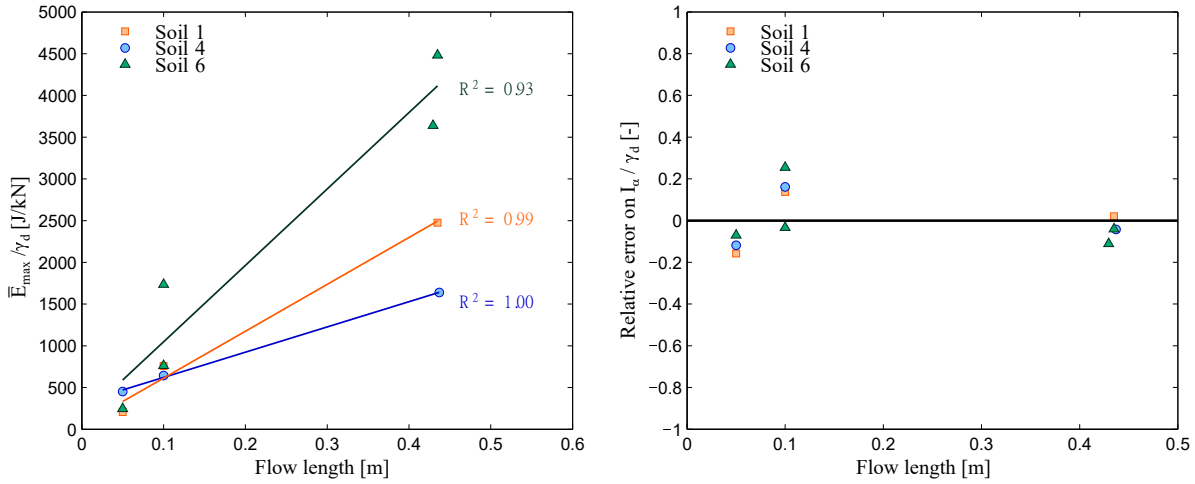

Figure 7: For all specimens of soils 1, 4 and 6 (left) cumulative expended energy per unit volume and dry volumetric weight versus seepage length and (right) relative error on the suffusion resistance index scaled by the dry unit weight I_α/γ_d versus the seepage length.

The previous results support the assumption that I_α and $\bar{E}_{\max}$ are intrinsic parameters to a soil so that they will be used to describe the suffusion process up to the fully eroded state.

4. A description inspired from the energy-based approach

With the objective to model the development of the suffusion process, a constitutive relationship, inspired from the energy-based approach, is now presented. The proposed relationship aims to describe the suffusion process up to the fully eroded state characterized by I_α and $\bar{E}_{\max}$ [14]. Based on this repeatable stable state of erodibility, we propose a dimensionless power relation linking the volumetric cumulative eroded mass $\bar{m}_{\text{cum}}$ and the volumetric cumulative expended energy $\bar{E}_{\text{cum}}$,

$$\frac{\bar{m}_{\text{cum}}(t_i) - \bar{m}_{\text{sat}}}{\bar{m}_{\max} - \bar{m}_{\text{sat}}} = \left(\frac{\bar{E}_{\text{cum}}(t_i)}{\bar{E}_{\max}} \right)^{b(t_i)} , \tag{4}$$

in which $b(t_i)$ is a parameter that controls the kinetics of suffusion and $\bar{m}_{\text{sat}}$ is the volumetric eroded mass lost during the saturation. Since $\bar{m}_{\text{sat}}$ is initially measured, it can be considered as a known parameter. The relationship (4) has been plotted in Figure 8 for all the specimens of soil 6 to illustrate the variability of the kinetics from one specimen to the other. Large values of $b(t_i) > 1$ implies a rather slow kinetics and conversely for $b(t_i) < 1$. It should be noted that the dotted lines do no render the instantaneous kinetics but rather an overall behaviour.

Experimentally, the erosion rate has been observed to be large at the beginning of each loading step and to decrease during the step [32, 5]. Hence, we expect $b(t_i)$ to vary accordingly. By looking at eq. (4), the definition of $b(t_i)$ is bonded by two constraints: (i) $b(t_i)$ should be a dimensionless variable, and (ii) the cumulative eroded mass should never decrease to remain physically admissible. By following the spirit of the energy approach, $b(t_i)$ is defined as a function of the power expended by flow P_{flow} and of a smoothed version of this power denoted P_{smoothed},

$$b(t_i) = \frac{P_{\text{smoothed}}(t_i)}{P_{\text{flow}}(t_i)} . \tag{5}$$

The smoothed power is determined based on a weighted moving average method,

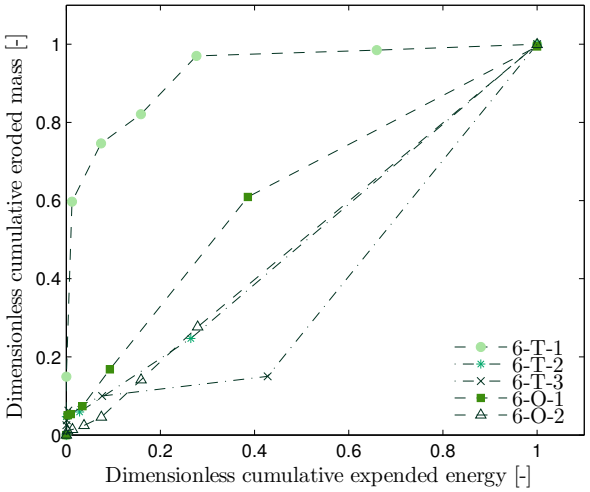

Figure 8: Dimensionless representation of the cumulative eroded mass with respect to the cumulative expended energy for all the specimens of soil 6.

$$P_{\text{smoothed}}(t_i) = \frac{kP_{\text{flow}}(t_i) + (k-1)P_{\text{flow}}(t_{i-1}) + ... + P_{\text{flow}}(t_{i-k})}{k + (k-1) + ... + 1}\,. \tag{6}$$

in which k corresponds to the number of values used to perform the smoothing. With time series data, the number of values k corresponds to a time upon which the smoothing is performed. In a sense, $b(t_i)$ is designed to identify higher frequency components on the signal of the power expended by flow P_{flow}. The physical constraint on the cumulative eroded mass $\bar{m}_{\text{cum}}(t_i) \geq \bar{m}_{\text{cum}}(t_{i-1})$ brings an additional constraint on the kinetics parameter,

$$\begin{aligned} &b(t_i) \geq b^*(t_i) \quad \text{with} \\ &b^*(t_i) = b(t_{i-1}) \frac{\log\left(\bar{E}_{\text{cum}}(t_{i-1})/\bar{E}_{\max}\right)}{\log\left(\bar{E}_{\text{cum}}(t_i)/\bar{E}_{\max}\right)}\,. \end{aligned} \tag{7}$$

In the end, at each instantaneous time t_i, the right-hand-side of eq. (5) is computed. The result is next checked by use of eq. (7). If admissible, the result is kept, if not the right-hand-side term of eq. (7) is taken instead:

$$\begin{aligned} &\text{if} \quad \frac{P_{\text{smoothed}}(t_i)}{P_{\text{flow}}(t_i)} \geq b^*(t_i) \;\rightarrow\; b(t_i) = \frac{P_{\text{smoothed}}(t_i)}{P_{\text{flow}}(t_i)} \\ &\text{if} \quad \frac{P_{\text{smoothed}}(t_i)}{P_{\text{flow}}(t_i)} < b^*(t_i) \;\rightarrow\; b(t_i) = b^*(t_i)\,. \end{aligned} \tag{8}$$

The specimen 6-T-2 is chosen to illustrate the above developments (Figure 9). The time series of the power and the smoothed power are plotted in Figure 9-left with a smoothing time of 10 seconds. The time series of the ratio between these two variables and the kinetics parameter $b(t_i)$ are illustrated in Figure 9-right. The $b(t_i)$ parameter decreases sharply at the beginning of each step and increases gently until the next hydraulic loading event. Initially, the $b(t_i)$ parameter is arbitrarily fixed to 2, which represents a very slow kinetics. This value is not of great importance as long as it is large enough not to influence the eroded mass prediction.

Finally, by combining eqs. (4) to (8), the cumulative eroded mass can be computed at any time. Three parameters are required: the erosion resistance index I_α, the maximum volumetric cumulative expended

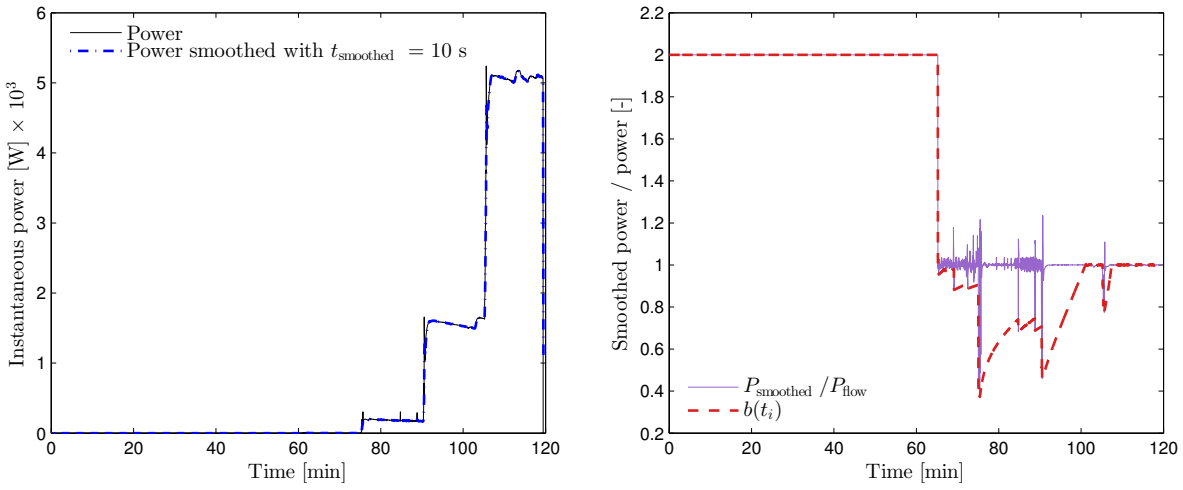

Figure 9: Illustrations of (left) the power expended by the flow $P_{\text{flow}}(t_i)$ and the smoothed version of this power $P_{\text{smoothed}}(t_i)$, and (right) of the ratio between $P_{\text{smoothed}}(t_i)/P_{\text{flow}}(t_i)$ and of the kinetics parameter $b(t_i)$ for the specimen 6-T-2.

energy $\bar{E}_{\max}$ and the number of values k used to perform the smoothing of $P_{\text{smoothed}}(t_i)$. In fact, k will be replaced by the smoothing time $t_{\text{smoothed}} = t_i - t_{i-k}$ which highlights its physical meaning.

To assess the validity of the description proposed, the cumulative eroded mass deducted from eqs. (4) to (8) is compared with that measured during laboratory tests, in Fig. 10 and 11 for soils 1, 4 and 6, respectively. The smoothing time t_{smoothed} has been fitted from tests 1-T-1 and 4-T-2 for the soils 1 and 4 ($t_{\text{smoothed}} = 60\,\text{s}$) and from test 6-O-2 for the soil 6 ($t_{\text{smoothed}} = 10\,\text{s}$), other tests constituting consequently validation cases. In addition, a sensitivity analysis is proposed in Section 5 to investigate the physical implication of this smoothing time.

Concerning soil 6, the proposed description is able to capture very well the experimental behaviour of the suffusion process for the calibration test 6-O-2 but also for the other validation tests, which are characterised by various sizes and hydraulic loading histories. However, the prediction proposed is not totally in agreement with the experimental data, in particular for specimens 6-T-1 and 6-O-1. For the former, the hydraulic conductivity decreases from initially around 4×10^{-4} m/s to 3×10^{-5} m/s at the end of the test (Fig. 5b). This decrease is inversely proportional to the increase of the characteristic time of diffusion which should also increase the characteristic time of suffusion. Recall that suffusion represents three coupled processes : detachment, transport and partial filtration of the fine fraction. Hence, the smoothing time which controls the kinetics of suffusion might be underestimated to accurately represent the late behavior of this specimen. Regarding specimen 6-O-1, the slight discrepancy between the prediction and the experimental data may be attributed to some fines particles that were dislodged during the saturation process and that exited the specimen during the very first minutes of the test. This assumption is supported by the fact that no strong power increase was measured while some mass was eroded.

Concerning the soils 1 and 4, the description proposed is able to capture very well the experimental behaviour of the suffusion process for both calibration tests 1-T-1 and 4-T-2. It is also able to capture fairly well the main features of the erosion process for specimens 1-T-2, 1-O-1 and 4-O-1. Sole, the prediction of 4-T-1 displays a quite large discrepancy with the experimental data. Alike specimen 6-O-1, we believe that some fines particles have been dislodged during the saturation phase (upward flow) and exited the sample right after the beginning of the test, i.e. right after the application of a small downward seepage flow.

The prediction capabilities of the energy-based relationship (4) were compared with that of two other constitutive relationships inspired from the shear stress-based approach and the power-based approach in Kodieh et al. [14]. While both the energy-based and the power-based relationships provided satisfactory predictions, the shear stress-based relationship tend to overestimate the development of the process. The

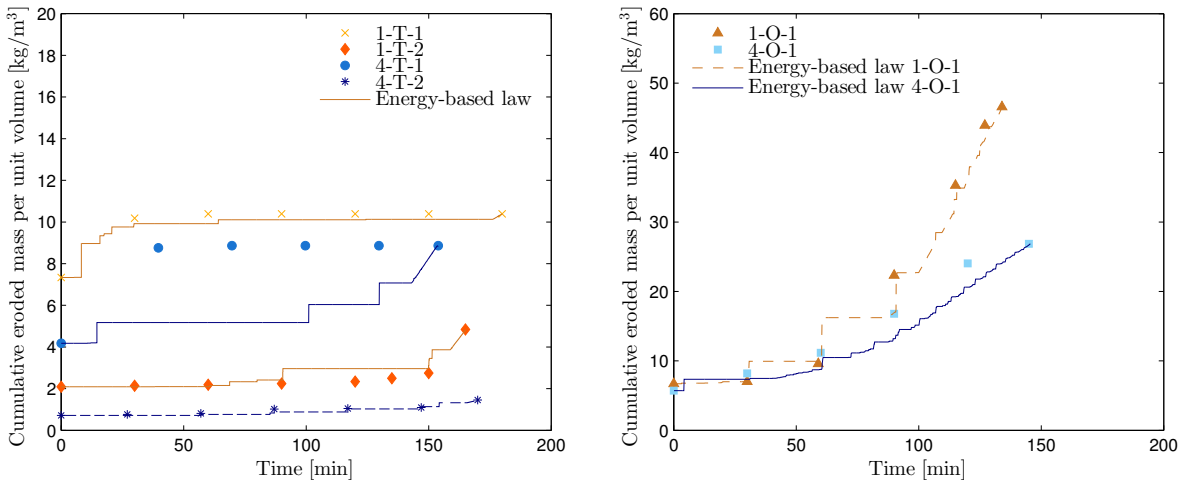

Figure 10: Comparison of the time evolution of the volumetric cumulative eroded mass for soils 1 and 4, between laboratory tests (symbols) and simulated data (lines). The smoothing time is equal to 60 seconds.

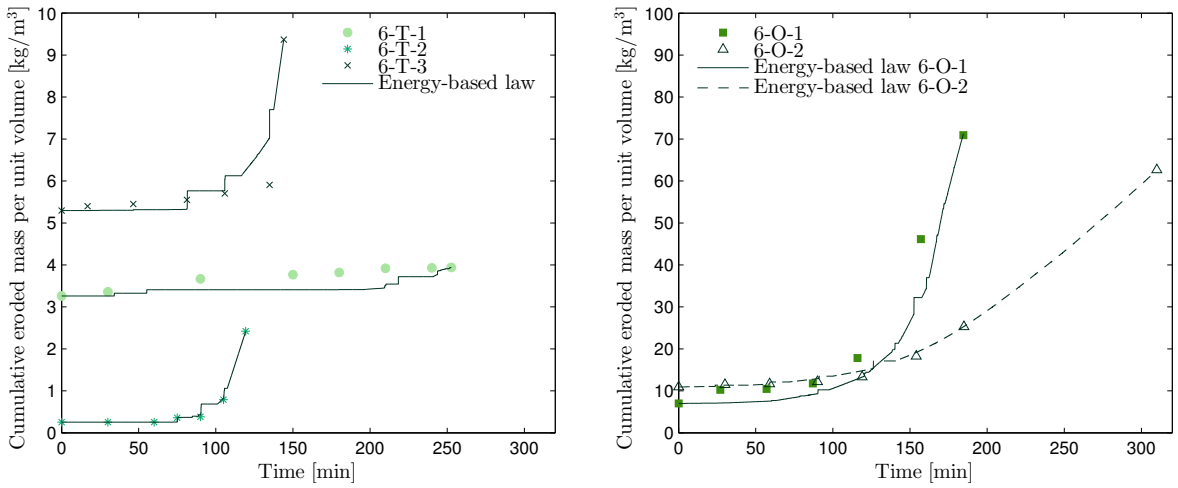

Figure 11: Comparison of the time evolution of the volumetric cumulative eroded mass for soil 6, between laboratory tests (symbols) and simulated data (lines). The smoothing time is equal to 10 seconds.

main advantages of the energy-based approach are its structural independence towards the hydraulic loading path and the careful study of the sensitivity of the introduced parameters towards the seepage length. Advantages and drawbacks of each approach, and modeling implications are further detailed in works [10, 14].

5. Sensitivity analysis on the suffusion kinetics parameter

The influence of the smoothing time in the range $3\,\mathrm{s} \leq t_{\mathrm{smoothed}} \leq 2\,\mathrm{min}$ is illustrated in Fig. 12 for the specimen 6-T-2. When this smoothing time is increased, the size of the peaks on the kinetics parameter $b(t_i)$ are increased. Hence, the values of the kinetics parameter $b(t_i)$ are lowered which induce a faster kinetics of the eroded mass towards the fully eroded state.

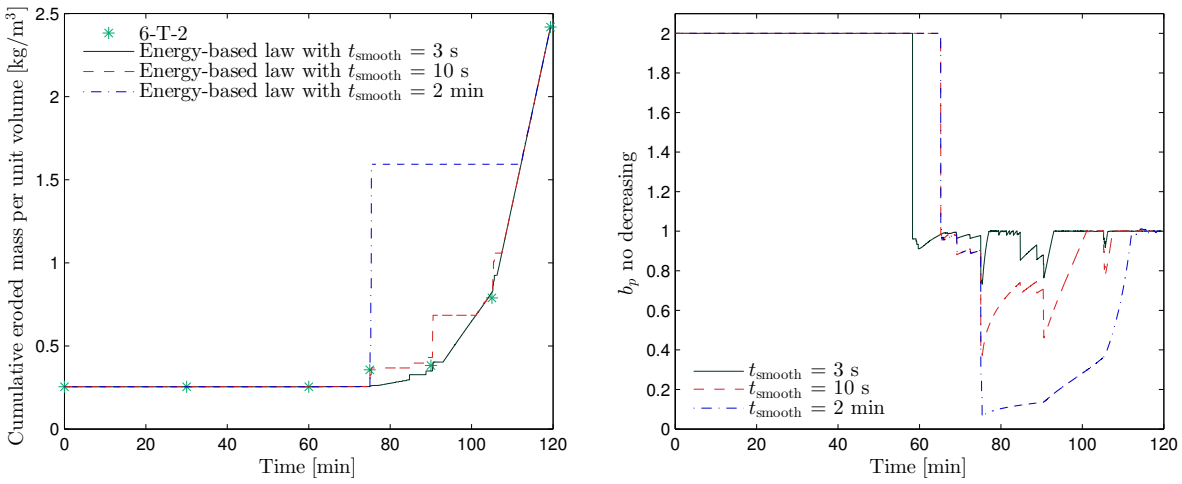

Figure 12: Influence of the smoothing time t_{smoothed} on (left) the time evolution of the cumulative volumetric eroded mass and (right) the kinetics parameter b.

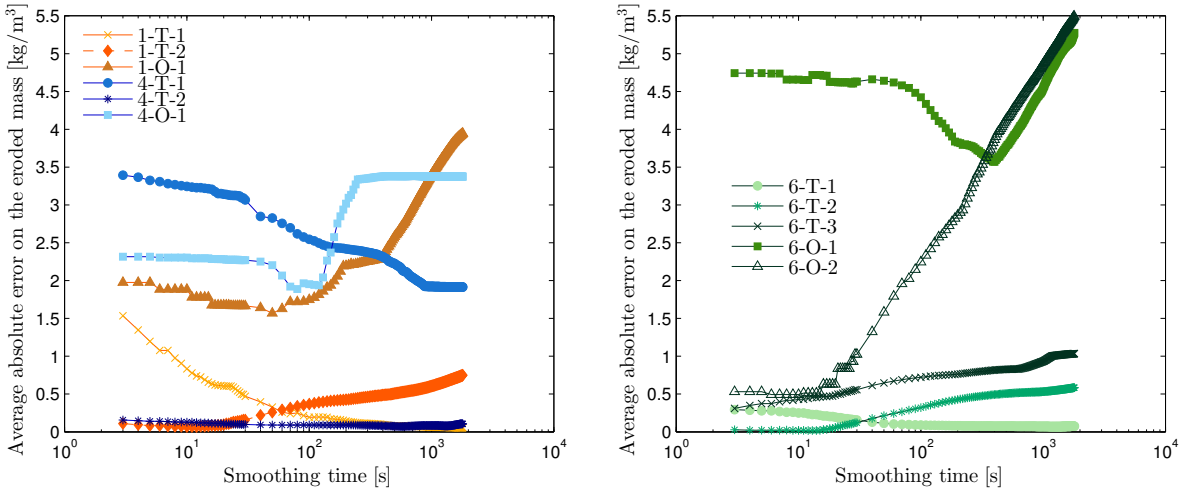

Figure 13: Influence of the smoothing time t_{smoothed} on the average absolute error for the tested specimens of (left) soils 1 and 4, and (right) soil 6.

To investigate further the influence and the physical meaning of the smoothing time, the average absolute error is computed for each tested specimen. In other words, the absolute error is computed for each experimental measure of the eroded mass, for ex. six absolute errors are computed for specimen 6-T-2; and the mean of these values is observed to objectively assess the performance of the simulation.

These average absolute errors are computed for several smoothing times, in the range $3\,\text{s} \leq t_{\text{smoothed}} \leq 30\,\text{min}$, and for all the specimens (Fig. 13). The lower smoothing time boundary is constrained by the acquisition frequency; while the upper smoothing time boundary is arbitrary restricted by the mean size of the loading stages (Figs. 5 and 4).

Among the eleven tested specimens, seven display a clear minimum average absolute error for a particular smoothing time: 1-T-2, 1-O-1, 4-T-2, 4-O-1, 6-T-2, 6-O-1 and 6-O-2. Three display a decreasing average absolute error : 1-T-1, 4-T-1 and 6-T-1 suggesting that large values of the smoothing time are more suitable.

Table 3: Diffusion characteristics of the tested specimens.

Test name	Initial specimen length (mm)	$\tilde{K}_F$ (m/s)	$\tilde{t}_{\text{diff}}$ (s)
1-T-1	50	1.93×10^{-5}	0.0627
1-T-2	100	1.20×10^{-3}	0.0040
1-O-1	435	1.38×10^{-2}	0.0066
4-T-1	50	2.41×10^{-4}	0.0050
4-T-2	100	6.60×10^{-4}	0.0073
4-O-1	437	3.54×10^{-2}	0.0026
6-T-1	50	6.79×10^{-6}	0.1756
6-T-2	100	1.36×10^{-4}	0.0356
6-T-3	100	9.79×10^{-3}	0.0050
6-O-1	430	4.20×10^{-3}	0.0213
6-O-2	435	3.60×10^{-3}	0.0255

Note: $\tilde{K}_F$ = average hydraulic conductivity; $\tilde{t}_{\text{diff}}$ = average characteristic diffusion time

Only 6-T-3 displays an increasing average absolute error which suggests that 3 s is the best-fit smoothing time for this specimen.

To highlight a possible correlation between the smoothing time and the characteristic diffusion time, a range of best-fit smoothing times is selected for each specimen: these smoothing times permit to limit the average absolute error of the cumulative eroded mass per unit volume ≤ 0.3 kg/m^3. For the specimen 6-T-2, the minimum average absolute error is equal to 0.017 kg/m^3 for a smoothing time of 13 seconds. The best-fit smoothing times range between 3 seconds and 90 seconds since they correspond to average absolute errors that are all below 0.3017 kg/m^3.

The characteristic diffusion time is proportional to the square of the seepage length L and to the inverse of the hydraulic diffusivity α_H [9],

$$t_{\text{diff}} = \frac{L^2}{\alpha_H} \,. \tag{9}$$

Assuming that the interstitial fluid and the grains are incompressible, the hydraulic diffusivity α_H can be expressed as a function of the Young's modulus E, the Poisson's ratio ν, the hydraulic conductivity K_F, the fluid density ρ_F and the gravity component g [9]:

$$\alpha_H = \frac{K_F}{\rho_F g} \frac{E(1-\nu)}{(1+\nu)\,(1-2\nu)} \,. \tag{10}$$

For the soils and tests at hand, we considered the Young's modulus $E = 2000$ MPa, the Poisson's ratio $\nu = 0.3$ and the fluid density $\rho_F = 1000$ kg/m^3. Since the hydraulic conductivity varies during each suffusion test, the average hydraulic conductivity $\tilde{K}_F$ over each test was chosen to compute an average diffusion time $\tilde{t}_{\text{diff}}$ (Table 3).

This average diffusion time was plotted against the range of best-fit smoothing times in Fig. 14 for all specimens except for 6-O-1 and 4-T-2. 6-O-1 is characterized with relatively large average absolute errors > 3 kg/m^3 irrespective of the smoothing time; while the predictions of 4-T-2 are rather insensitive to the smoothing time, probably because very little mass is being eroded. Also on Fig. 14 approximate tendencies are presented with discontinuous lines. We observe that, for each soil, the best-fit smoothing times are larger when the average diffusion time is large. A large average diffusion time implies either a long seepage length or a low hydraulic conductivity (specimens 1-T-1 and 6-T-1). In those cases, the suffusion kinetics tends to

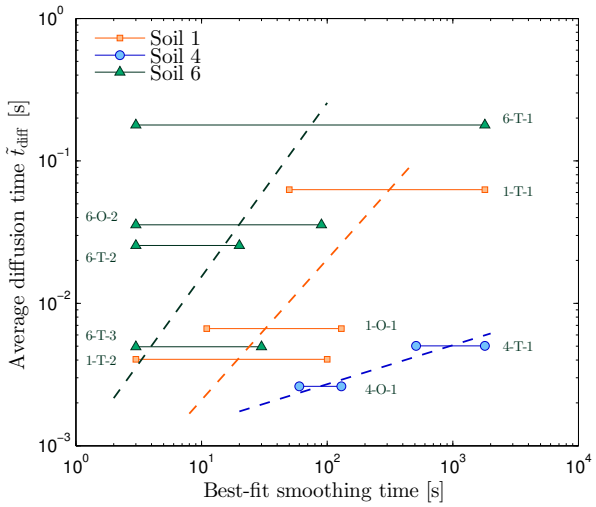

Figure 14: Average diffusion time $\tilde{t}_{\text{diff}}$ versus the best-fit smoothing time range for all tested specimens, except 6-O-1 and 4-T-2. Approximate tendencies are presented with discontinuous lines. All the smoothing times corresponding to average absolute errors ≤ 0.3 kg/m^3 above the minimum absolute error have been considered as best-fit smoothing times for each specimen.

be fast because detachment and transport of the fine particles are quickly dominated by a clogging process. Hence, most of the events arise in the early times of the test. On the other hand, a low average diffusion time indicates either a small seepage path or a large hydraulic conductivity. Because of this lower retention time, detachment and transport usually prevails upon clogging with is either unstable or in-existent. For each soil, the suffusion kinetics tends to be slower because the suffusion of the fine particles require a larger hydraulic loading to develop, which is applied towards the end of each test (specimens 1-T-2, 1-O-1, 4-T-1, 4-O-1, 6-T-2, 6-T-3, 6-O-2).

Interestingly, for low average diffusion times, the best fit smoothing times tend to decrease with the increase of the initial fine content (Fig. 3). In other words, the suffusion kinetics tends to get slower when the initial percentage of fine particle increases. Indeed, more fine particles require larger hydraulic loadings for the detachment and transportation to reach a fully eroded state.

In the light of the tendencies suggested by Fig. 14, one may assume that the instantaneous smoothing time should be related to the instantaneous diffusion time by a power law,

$$t_{\text{smoothed}} = (B \times t_{\text{diff}})^A; \tag{11}$$

in which the coefficients A and B are deduced from the tendencies drawn in Figure 14 (see Table 4).

The eroded mass predictions using this new assumption are displayed in Figs. 15 and 16. This assumption degrades slightly the prediction for one tests : 4-O-1 (see Table 5). On the other hand, an improved or equal prediction is obtained for the other ten specimens 1-T-1, 1-T-2, 1-O-1, 4-T-1, 4-T-2, 6-T-1, 6-T-2, 6-T-3, 6-O-1 and 6-O-2, which strengthens the idea that the kinetics of suffusion should be linked to the hydraulic diffusion time.

6. Conclusion

Suffusion mechanism that can take place within hydraulic embankments is a complex phenomenon that calls for non-linear behaviour laws. Consequently, computing the cumulative eroded mass with time is an important step to understand and model the suffusive hydro-mechanical behaviour of soils. In this paper, a new phenomenological relationship based on the energy approach, initially developed by Marot et al. [19], has been proposed to predict the time evolution of the cumulative eroded mass. This relationship uses only

Table 4: Coefficients used to relate the smoothing time with the diffusion time based on eq. (11).

Soil gradation	A	B
1	1.0134	4627.01
4	3.6523	1303.47
6	0.8194	1079.94

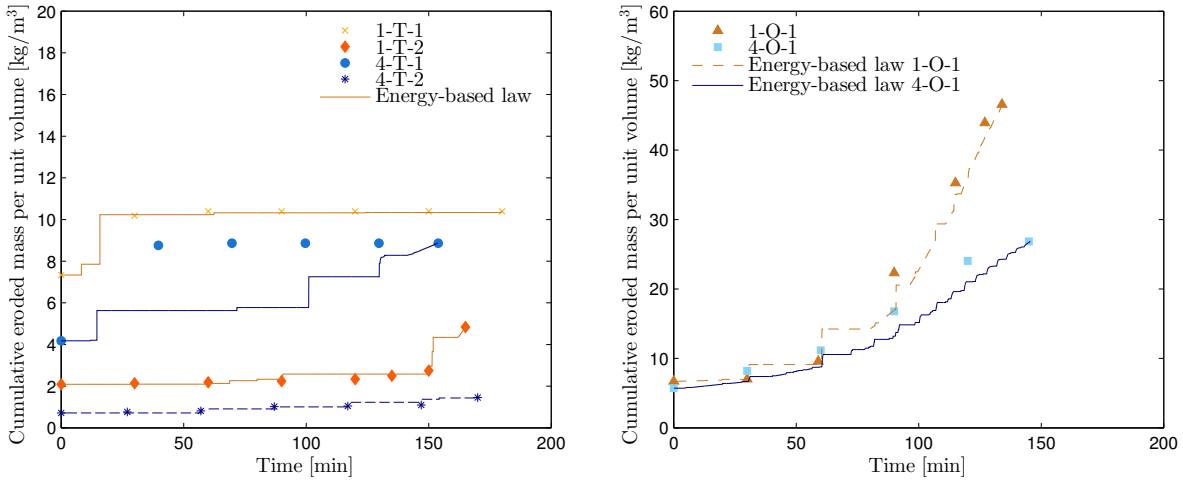

Figure 15: Comparison of volumetric cumulative eroded mass for soils 1 and 4, between laboratory tests (symbols) and simulated data (lines). The instantaneous smoothing time is related to the instantaneous diffusion time based on eq. (11) and Table (4).

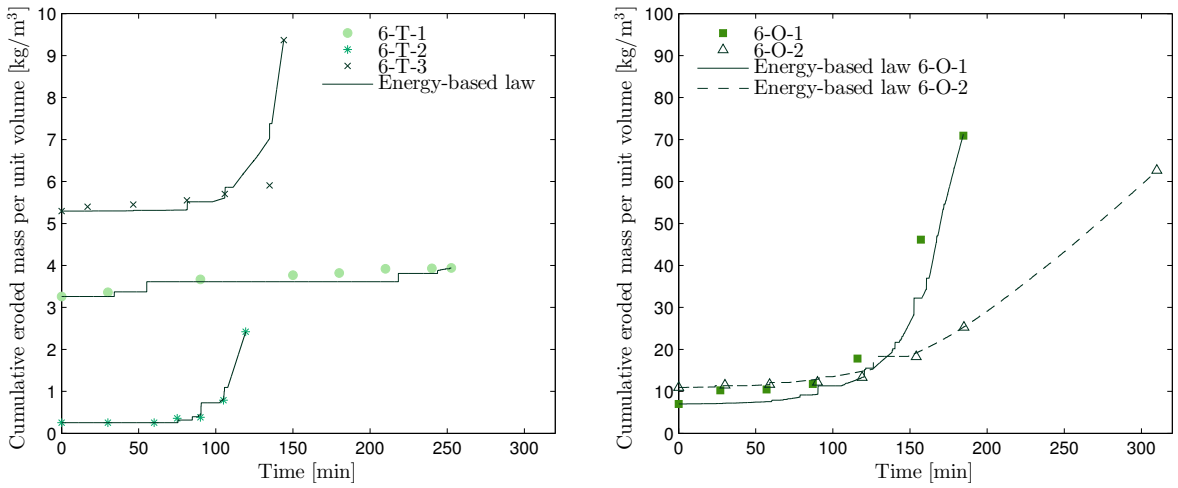

Figure 16: Comparison of volumetric cumulative eroded mass for soil 6, between laboratory tests (symbols) and simulated data (lines). The instantaneous smoothing time is related to the instantaneous diffusion time based on eq. (11) and Table (4).

three variables: the erosion resistance index I_α, the maximum volumetric cumulative energy $\bar{E}_{\max}$ and the

Table 5: Comparison of average absolute errors for each specimens with a constant smoothing time (10 s for soil 6 and 60 s for soils 1 and 4) and with a variable smoothing time based on eq. (11) and Table (4).

Test name	Average absolute errors [kg/m^3] with a constant smoothing time		with a variable smoothing time
1-T-1	0.264	$\searrow$	0.066
1-T-2	0.291	$\searrow$	0.099
1-O-1	1.627	$\searrow$	1.589
4-T-1	2.757	$\searrow$	2.213
4-T-2	0.091	$\rightsquigarrow$	0.095
4-O-1	2.067	$\nearrow$	2.124
6-T-1	0.251	$\searrow$	0.135
6-T-2	0.02	$\rightsquigarrow$	0.033
6-T-3	0.431	$\searrow$	0.331
6-O-1	4.657	$\rightsquigarrow$	4.641
6-O-2	0.493	$\rightsquigarrow$	0.497

smoothing time t_{smoothed}. To summarize, our approach relies on four mains points:

- The stable state of erodibility is considered to be intrinsic to a soil. Upon applying a multi-step hydraulic loading, this state is reached when the hydraulic conductivity remains constant and the erosion rate decreases significantly. This state is characterized by the erosion resistance index I_α and the maximum volumetric cumulative energy $\bar{E}_{\max}$.
- The maximum volumetric cumulative energy $\bar{E}_{\max}$ scaled by the dry density increases with the seepage length.
- The kinetics of the suffusion process is controlled by the power dissipated by the flow P_{flow} and by the smoothing time t_{smoothed}.
- Our results suggest that the kinetics of suffusion should be linked to the kinetics of hydraulic diffusion. This is due to the fact that experimentally measured suffusion (eroded particles reaching the outlet of a specimen) involves subsequent and rapidly simultaneous detachment, transportation and partial re-deposition of the fines particles.

The presented phenomenological relationship is compared against eleven suffusion tests performed on three gap-graded soils. The experimental campaign uses two apparatuses: a large oedo-permeameter device and a smaller triaxial-permeameter (used in oedometric conditions) so that three seepage lengths have been investigated ranging from 50 mm to 437 mm. The hydraulic loading is applied in the form of a multi-step hydraulic gradient with different amplitudes and step durations. The energy-based relationship was able to capture fairly well the experimentally measured suffusion for ten specimens and the main tendency for the last one.

The process of measuring the stable state of erodibility should be improved to target a better accuracy of the erosion resistance index I_α and of the maximum volumetric cumulative energy $\bar{E}_{\max}$. The linear tendency obtained between the maximum volumetric cumulative energy $\bar{E}_{\max}$ scaled by the dry unit weight and the seepage length should be confirmed for additional types of gradings and seepage lengths. Nevertheless, this new relationship is promising and leads to a useful description of the eroded mass for the specimens involved in this study. It requires at least one multi-step test up to the stable state of erosion, for two seepage lengths, to measure and calibrate all the parameters. Such approach may then be used in continuum models which tackles the hydro-mechanical behavior of suffusive soils [10].

Acknowledgments

The authors want to thank the french company Electricité De France - Centre d'Ingénierie Hydraulique (EDF-CIH) for the financial support provided for this study.

Data Availability Statement

The data that support the findings of this study are available from the corresponding author upon reasonable request.

References

[1] Aboul Hosn, R., Sibille, L., Benahmed, N. and Chareyre, B., A discrete numerical model involving partial fluid-solid coupling to describe suffusion effects in soils, Computers and Geotechnics, 95, 30-39, 2018.
[2] Ahmadi, M., Shire, T., Mehdizadeh, A. and Disfani, M., DEM modelling to assess internal stability of gap-graded assemblies of spherical particles under various relative densities, fine contents and gap ratios, Computers and Geotechnics, 126, 103710, 2020.
[3] Bendahmane, F., Marot, D. and Alexis, A., Experimental parametric study of suffusion and backward erosion, Journal of Geotechnical and Geoenvironmental Engineering, 134(1), 57-67, 2008.
[4] Bui, T.-A., Gelet, R. and Marot, D., Modelling of internal erosion based on mixture theory, International Journal of Numerical and Analytical Methods in Geomechanics, 43(15), 2407-2430,2019.
[5] Chang, D.S. and Zhang, L.M., Critical hydraulic gradients of internal erosion under complex stress states, Journal of Geotechnical and Geoenvironmental Engineering, 139(9), 1454-1467, 2013.
[6] Chang, D.S. and Zhang, L.M., Extended internal stability criteria for soils under seepage, Soils and Foundations, 53(4), 569-583, 2013.
[7] Chang, DS and Zhang, LM, A stress-controlled erosion apparatus for studying internal erosion in soils, Geotechnical Testing Journal, 34(6), 579-589, 2011.
[8] Fell, R. and Fry, J.-J., Internal erosion of dams and their foundations: selected and reviewed papers from the workshop on internal erosion and piping of dams and their foundations, Aussois, France, 25–27 April 2005, CRC Press, 2014.
[9] Gelet, R., Loret, B. and Khalili, N., Thermal recovery from a fractured medium in local thermal non-equilibrium, International Journal for Numerical and Analytical Methods in Geomechanics, 37(15), 2471-2501, 2013.
[10] Gelet, R., Kodieh, A., Marot, D. and Nguye,n N., Analysis of volumetric internal erosion in cohesionless soils: model, experiments and simulations, International Journal for Numerical and Analytical Methods in Geomechanics, DOI: NAG-20-0329.R1, 2021.
[11] Indraratna, B., Israr, J. and Rujikiatkamjorn, C., Geometrical method for evaluating the internal instability of granular filters based on constriction size distribution, Journal of Geotechnical and Geoenvironmental Engineering, 141(10), 04015045, 2015.
[12] Ke, Lin and Takahashi, Akihiro, Drained monotonic responses of suffusional cohesionless soils, Journal of Geotechnical and Geoenvironmental Engineering, 141(8), 04015033, 2015.
[13] Kenney, T.C. and Lau, D., Internal stability of granular filters, Canadian Geotechnical journal, 22(2), 215-225, 1985.
[14] Kodieh, A., Gelet, R., Marot, D. and Fino, A.Z., A study of suffusion kinetics inspired from experimental data: comparison of three different approaches, Acta Geotechnica, 16(2), 347-365, 2021.
[15] Le, V.T., Development of a new device and statistical analysis for characterizing soil sensibility face suffusion process, Université de Nantes, 2017.
[16] Le, V.T., Marot, D., Rochim, A., Bendahmane, F. and Nguyen, H.H., Suffusion susceptibility investigation by energy-based method and statistical analysis, Canadian Geotechnical Journal, 55(1), 57-68, 2017.
[17] Li, M. and Fannin, R.J., Comparison of two criteria for internal stability of granular soil, Canadian Geotechnical Journal, 45(9), 1303-1309, 2008.
[18] Marot, D. and Benamar, A. Erosion of geomaterials. Chapter 2: Suffusion, transport and filtration of fine particles in granular soil, ISTE Ldt. & John Wiley & Sons, 2012.
[19] Marot, D., Le, V.D., Garnier, J., Thorel, L. and Audrain, P., Study of scale effect in an internal erosion mechanism: centrifuge model and energy analysis, European Journal of Environmental and Civil Engineering, 16(1), 1-19, 2012.
[20] Marot, D., Rochim, A., Nguyen, H.-H., Bendahmane, F. and Sibille, L., Assessing the susceptibility of gap-graded soils to internal erosion: proposition of a new experimental methodology, Natural Hazards, 83(1), 365-388, 2016.
[21] Moffat, R. and Fannin, R.J., A hydromechanical relation governing internal stability of cohesionless soil, Canadian Geotechnical Journal, 48(3), 413-424, 2011.
[22] Muir Wood, D. and Maeda, K. and Nukudani, E., Modelling mechanical consequences of erosion, Géotechnique, 60(6), 447-457, 2010.
[23] Perzlmaier, S., Muckenthaler, P. and Koelewijn, A.R., Internal erosion of dams and their foundations : selected and reviewed papers from the workshop on internal erosion and piping of dams and their foundations, Aussois, France, 25-27 April 2005, CRC Press, 179-190, 2014.

[24] Reddi, L.N., Lee I.-M. and Bonala M.V., Comparison of internal and surface erosion using flow pump tests on a sand-kaolinite mixture, Geotechnical Testing Journal, 23(1), 116-122, 2000.
[25] Rochim, A., Characterization of suffusion susceptibility of granular soils, Université de Nantes, 2015.
[26] Rochim, A., Marot, D., Sibille, L. and Le V.T., Effects of hydraulic loading history on suffusion susceptibility of cohesionless soils, Journal of Geotechnical and Environmental Engineering, 7(1143), 04017025, 2017.
[27] Rousseau, Q., Sciarra, G., Gelet, R. and Marot, D., Constitutive Modeling of a Suffusive Soil with Porosity-Dependent Plasticity, European Working Group on Internal Erosion, Springer, Cham 168-179, 2018.
[28] Rousseau, Q., Sciarra, G., Gelet, R., Marot, D., Modelling the poroelastoplastic behaviour of soils subjected to internal erosion by suffusion, International Journal for Numerical and Analytical Methods in Geomechanics, 44(1), 117-136, 2020.
[29] Sail, Y., Marot, D., Sibille, L., and Alexis, A., Suffusion tests on cohesionless granular matter: Experimental study, European Journal of Environmental and Civil Engineering, 15(5), 799-817, 2011.
[30] Scholtès, L., Hicher, P.-Y. and Sibille, L., Multiscale approaches to describe mechanical responses induced by particle removal in granular materials, Comptes Rendus Mécanique, 338(10-11), 627-638, 2010.
[31] Shire, T., O'Sullivan, C., Hanley, K.J. and Fannin, R.J., Fabric and effective stress distribution in internally unstable soils, Journal of Geotechnical and Geoenvironmental Engineering, 140(12), 04014072, 2014.
[32] Sibille, L., Marot, D. and Sail Y., A description of internal erosion by suffusion and induced settlements on cohesionless granular matter, Acta geotechnica, 10(16), 735-748, 2015.
[33] Sibille, L., Lominé, F., Poullain, P., Sail, Y., and Marot, D., Internal erosion in granular media: direct numerical simulations and energy interpretation, Hydrological Processes, 29(9), 2149-2163, 2015.
[34] Sterpi, Donatella, Effects of the erosion and transport of fine particles due to seepage flow, International Journal of Geomechanics, 3(1), 111-122, 2003.
[35] Wan, C.F. and Fell, R., Journal of Geotechnical and Geoenvironmental Engineering, Assessing the potential of internal instability and suffusion in embankment dams and their foundations, 134(3), 401-407, 2008.
[36] Yan, L., Li, M. and Anderlini, C., Assessment of Internal Erosion of Zoned Embankment Dams with Widely Graded Materials, European Working Group on Internal Erosion, Vancouver, BC, Canada, 18-21th of June, 2019.
[37] Yang, J., Yin, Z.-Y. and Laouafa, F., Hicher, P.-Y., Internal erosion in dike-on-foundation modeled by a coupled hydromechanical approach, International Journal for Numerical and Analytical Methods in Geomechanics, 43(3), 663-683, 2019.
[38] Zhang, L., Gelet, R., Marot, D., Smith, M., Konrad, J.-M., A method to assess the suffusion susceptibility of low permeability core soils in compacted dams based on construction data, European Journal of Environmental and Civil Engineering, 23(5), 626-644, 2019.
[39] Zhang, X., Wong, H., Leo, C.J., Bui, T.A., Wang, J., Sun W. and Huang Z., A thermodynamics-based model on the internal erosion of earth structures, Geotechnical and Geological Engineering, 31(12), 479-492, 2013.
[40] Zhong, C., Le, V.T., Bendahmane, F., Marot, D. and Yin Z.-Y., Investigation of spatial scale effects on suffusion susceptibility, Journal of Geotechnical and Geoenvironmental Engineering, 144(19), 04018067, 2018.